ELSEVIER

Catalysis Today 77 (2002) 225–235

CATALYSIS TODAY

www.elsevier.com/locate/cattod

Ni/SiO_2 and Fe/SiO_2 catalysts for production of hydrogen and filamentous carbon via methane decomposition

M.A. Ermakova*, D.Yu. Ermakov

Boreskov Institute of Catalysis, Siberian Branch of the Russian Academy of Sciences, Prospekt Ak. Lavrentieva 5, Novosibirsk 630090, Russia

Abstract

High-loaded Ni–SiO_2 and Fe–SiO_2 catalysts (85–90 wt.% of metal) for methane decomposition were prepared by the heterophase sol–gel method and studied at various stages of their preparation and operation using XRD, IR, TPR, TEM techniques and the stoichiographic method of differentiating dissolution. Carbon yield was demonstrated to depend on the interaction between nickel and silica. The yield equal to 384 g C/g Ni was characteristic of the catalyst free of silicates, while the presence of silicates in amount of 1.5–2 wt.% caused a decrease in the carbon yield to 40 g C/g Ni. The effect of silicates comprised in iron catalysts is not so unambiguous as for nickel catalysts, they can both inhibit and promote the process of carbon formation.

Keywords: Sol–gel synthesis; Ni–SiO_2 and Fe–SiO_2 catalysts; Methane decomposition; Carbon yield

1. Introduction

Direct catalytic cracking of hydrocarbons is a promising process for industrial processing of natural and associated oil gases. Methane is the main component of these gases. Therefore, metal-catalyzed decomposition of methane at moderate temperatures is of most practical importance. Two products of methane decomposition, molecular hydrogen and filamentous carbon, are produced by direct catalytic cracking. The hydrogen is free of carbon monoxide. The presence of CO is often undesirable or even inadmissible, for example, due to catalyst poisoning in electrocatalytic cells with hydrogen used as fuel [1,2].

The not separated mixture of hydrogen and methane is more effective fuel for internal combustion engines and gas turbine power plants than natural or oil gas.

The second reaction product is nanofiber carbon. It is of interest as a very pure graphitized carbon material potentially applicable to various industrial processes. Growth of carbon filaments is a result of the following processes. Dissociative chemisorption of hydrocarbons produces carbon atoms, which are released on certain faces of a catalytic metal particle (e.g. Ni) and diffuse towards opposite faces where crystallize in the form of continuous graphite-like structures [3,4]. The rate of carbon deposition is controlled by isothermal carbon diffusion through the metal particle [5,6]. The catalyst is deactivated because of the active surface blocking by carbonaceous deposits [7].

Attention of numerous researchers was paid to carbon materials synthesized by cracking of various hydrocarbons due to their unique structure built-up by interlaced nanofibers or nanotubes. Properties of these materials were studied regarding their use as adsorbents [8], catalysts [9,10], catalyst supports [11,12] or

* Corresponding author.
E-mail address: erm@catalysis.nsk.su (M.A. Ermakova).

0920-5861/02/$ – see front matter
PII: S0920-5861(02)00248-1

for storage of hydrogen in hydrogen power engineering [13]. Some progress in the field was achieved.

It is evident that the practical importance of catalytic cracking of methane can only be provided by the use of deliberately designed highly effective catalysts. This is a rather complex problem, however. The efficiency here means a long catalyst lifetime even though carbon is deposited in large quantity. Nickel is the most active catalyst for decomposition of hydrocarbons including methane. However, nickel particles larger than 100 nm in size are incapable of producing filaments but covered by a crust which isolates them from the reaction medium. For this reason unsupported nickel powder, liable to strong sintering in hydrocarbon media, cannot produce carbon filaments [14]. Although the process of methane cracking does not need fine catalyst particles [15], the use of supported catalysts necessary. Cobalt is an inappropriate catalyst for methane decomposition due to its lower activity [16], and, in addition, the high price and toxicity. In contrast, iron-based catalysts, which are inexpensive, non-toxic and resistant to high temperatures [17], are attractive for the process. Moreover, carbon deposits synthesized with iron catalysts contain thin-wall nanotubes in large amount, which are the most valuable product among carbon nanofibers.

We have reported before that the carbon yield reached 384 g C/g Ni over 90% Ni–10% SiO_2 catalysts synthesized by the sol–gel method [15,18]. Carbon yield was much lower over Ni catalysts with other commonly used supports, such as alumina, zirconium oxide, magnesia and titanium oxide, even if the nickel particles were approximately equal in size in all reduced catalysts [15]. Interaction between the components was assumed to affect the catalytic properties of the systems.

Since silica was found the most suitable support of methane decomposition catalysts, the present work was aimed at study of the influence of silica on ability of the catalysts to accumulate carbon.

2. Experimental

2.1. Catalyst preparation

A nickel precursor was prepared by hydrolysis of the ammonia complex produced by dissolving nickel nitrate in aqueous ammonia solution. The precipitate was filtered out and washed with water in order to remove ammonium nitrate. The specific surface area of the prepared hydroxide (α-$Ni(OH)_2$) was 460 m^2/g after drying in air at 110 °C. Non-stoichiometric nickel oxide (63.3 wt.% Ni) was prepared by calcining nickel hydroxide in flowing air at 250 °C. The specific surface area of the oxide was 400 m^2/g. The texture of this nickel oxide was further varied by calcination at 350, 450 and 700 °C. Moisture capacity of nickel oxides was from 6 to 0.8 ml/g.

To prepare 90% Ni–10% SiO_2 systems, the samples of nickel oxide were modified with silica by mixing them with alcosol containing silica in a certain amount. Alcosol was prepared by mixing 50 ml of TEOS, 40 ml of ethanol, 2 ml of water and 0.5 ml of 40% HCl. Content of silica in the alcosol was 0.147 g per 1 ml and could be varied by dilution with ethanol. The mixture of NiO and alcosol was dried in flowing air at room temperature. Then the temperature was elevated to 150 °C and the sample was allowed to stand at this temperature for an hour. The next step was reduction in hydrogen at 550 °C.

Iron hydroxide prepared by precipitation of $FeCl_3 \cdot 6H_2O$ with an aqueous ammonia solution was used for synthesis of iron catalysts. The precipitate was carefully washed with water, then dried and calcined in a muffle furnace at 300 °C for 4 h. The texture of the prepared iron oxide ($Fe_2O_3 \cdot nH_2O$, $S_{specific} = 106\ m^2/g$) was varied by calcining it in air for an hour at different temperatures ranging from 450 to 800 °C. Moisture capacity of iron oxides was from 3.7 to 1 ml/g.

Iron catalysts were prepared by heterophase sol–gel method in the way similar to nickel catalysts. ($Fe_2O_3 + SiO_2$) systems were reduced by hydrogen at 700 °C.

2.2. Characterization of catalysts and carbon

Samples were reduced in the temperature-programmed reduction (TPR) mode using a quartz U-shaped reactor by heating from room temperature to 900 °C at the heating rate of 5 °C min^{-1}, in 10% (v/v) H_2 in argon (the gas mixture was dehydrated by KOH). The gas mixture flow rate was preset at 30 ml/min at atmospheric pressure. The sample weight was 6 mg.

Phase composition of samples was studied using X-ray powder diffraction technique. XRD patterns

were recorded using a URD-63 diffractometer (Cu Kα radiation at $\lambda = 0.15418$ nm, a graphite crystal monochromator). Silicon was used as the internal reference. Coherent scattering regions were determined by the Scherer equation based on half-widths of diffraction lines (1 1 1), (2 0 0) for nickel oxide and nickel metal and diffraction lines (1 0 4), (1 1 0) for α-Fe_2O_3 and (1 1 0) for α-Fe.

Infrared (IR) spectra were recorded (21 scans) at room temperature at the resolution of 4 cm^{-1} using a BOMEM-MB-102 and Specord spectrophotometers. Samples were finely ground and dispersed in KBr pellets with the ratio of about 1.5 mg per 500 mg of KBr.

Micrographs were recorded using transmission electron microscope JEM-100CX.

Textural parameters of samples were studied by low temperature adsorption of nitrogen at 77 K using an automated installation ASAP-2400 (Micrometrics).

Empirical formula and quantitative contents of individual phases in samples under study were determined by the method of differentiating dissolution [19]. The studies were carried out using a flow Teflon reactor. Mass of the samples was 5 mg. The solvent was passed at the rate of 3.65 ml/min. The dynamic dissolution regime implied variations in the solvent composition from H_2O (pH = 7) through H_2O:HCl (pH = 2) to H_2O:acids mixture = 10:1 (pH = 1.2 at the component ratio H_2SO_4:H_3PO_4:HNO_3:HF = 4:3:1:2). The dissolution process was conducted at linear temperature elevation at the rate of 1 °C/min. An inductively coupled plasma atomic emission spectrometer (PST of "Baird Europe", The Netherlands) was used as the analyzer detector.

2.3. Catalysts testing

The catalysts were tested using a laboratory installation with a vibrating flow quartz reactor. Nickel catalysts were reduced and tested at 550 °C, and iron catalyst at 700 °C. The working zone of the reactor was 10 cm^3. Load of catalysts was in amount of 10 mg on the basis of nickel or in amount of 15 mg on the basis of iron. High-purity methane (99.99%) was used for decomposition. Methane flow was 20 cm^3/min for Ni samples and at 12 cm^3/min for Fe samples. The hydrogen concentration in the mixture was determined using a chromatographic column filled with NaX zeolite. The amount of carbon deposited on the catalyst during the reaction time was determined by weighing unloaded samples.

The methane conversion was calculated by the formula:

$$X\,(\%) = \frac{1-c}{1+c} \times 100$$

3. Results and discussion

3.1. Nickel catalysts

A number of catalysts containing 90% of nickel are studied (Table 1). Tabulated data demonstrate that the carbon yield increases from 40 to 384 g C/g Ni and the lifetime from 4 to 50 h (Fig. 1) with a decrease in the specific surface area of nickel oxide used for catalyst preparation. Presumably, that occurs due to a lower proportion of silicates dissolved in the nickel particles. Among the catalysts under consideration, the oxide precursor of catalyst 1 has the maximal specific surface area equal to 400 m^2/g and, consequently, is the most reactive with respect to silica to form interphase silica-like compounds. Calcination of the precursor at 350 °C or higher temperatures results in a decrease in its specific surface area and, consequently, in lowering its ability to form interphase silica-like compounds.

In order to verify this assumption, catalysts 1 and 4 are thoroughly studied (Fig. 2a–d) at different stages of their preparation, as well as during the reaction of methane decomposition. Among the catalysts under

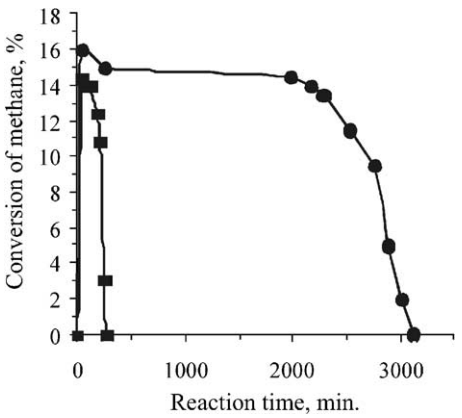

Fig. 1. Methane conversion over catalysts 1 (rectangles) and 5 (circles) depending on reaction time at 550 °C.

Table 1
Influence of the specific surface area of NiO on carbon yield over 90% Ni–10% SiO_2 catalysts

Sample	Temperature of calcination (°C)	Specific area of NiO (m^2/g)	Average size of Ni particles by XRD (nm)	Average size of Ni particles by TEM (nm)	Carbon yield (g C/g Ni)
1	250	400	7	6.8	40
2	350	144	10	9	300
3	450	56	17	16	375
4	700	7	60	62	384

study, the chosen samples provide extreme values of carbon yield.

Fig. 3 shows TPR profiles of samples 1 and 4 and, for comparison, TPR profiles of oxides used as precursors of these catalysts. One can see two peaks at 236 and 246 °C at reduction of silica-free dispersed nickel oxide. Notice that the first peak is only observed at reduction of NiO prepared at temperatures below 400 °C. It is Mile's opinion [20] that this effect is accounted for by the "Ni_2O_3" to NiO transition.

The process of Ni^{2+} to Ni^0 transition starts from the point of ca. 240 °C; it is observed within a very narrow temperature range between 240 and 255 °C. Even though the reduction temperature is low, nickel

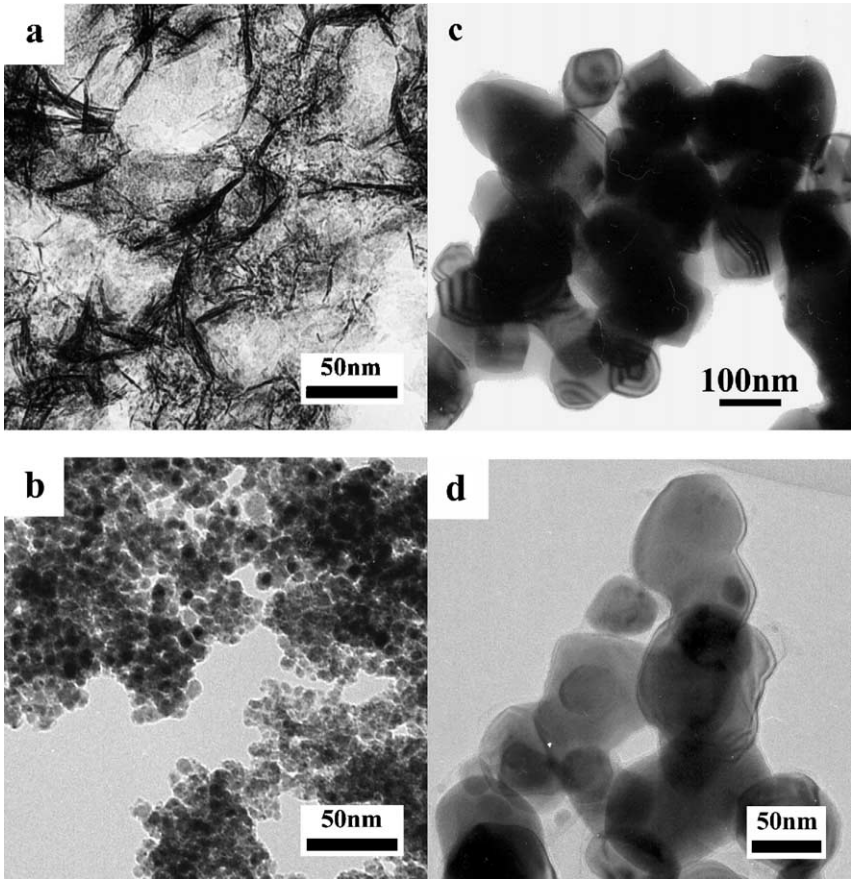

Fig. 2. Catalyst 1 in oxide form (a) and reduced form (b); catalyst 4 in oxide form (c) and reduced form (d).

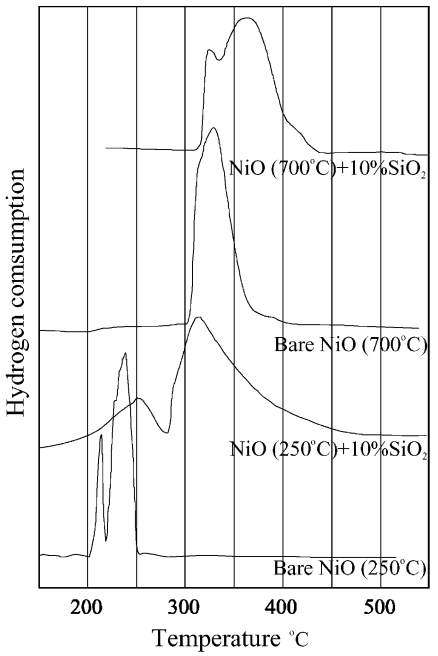

Fig. 3. TPR of the nickel oxides and oxide forms of catalysts 1 and 4.

crystallites increase in average size from 3–4 nm (initial oxide particles) to 44 nm (from XRD date). Analysis of the TPR profile obtained at reduction of sample 1 demonstrates that addition of SiO_2 results in a remarkable rise of the reduction temperature, as well as in broadening of the second peak of hydrogen consumption. A considerable decrease in the average size of nickel crystallites to 7 nm is indicated by XRD data (Table 1). Another evidence is provided by TEM studies (Fig. 2b).

A single peak from 300 to 380 °C with the maximum at 332 °C (Fig. 3) corresponds to reduction of the oxide precursor of sample 4 (Fig. 2c). This kind of reduction is characteristic of stoichiometric nickel oxide [21]. This oxide sample, when modified with silica, starts reducing at the same temperature but finishes at 450 °C, that is 70 °C higher than the complete reduction point of pure nickel oxide calcined at 700 °C. Splitting of the peak into two peaks with maxima at 335 and 370 °C is also observed. The first maximum can be attributed to reduction of silica-free NiO, while the second characterizes reduction of silica–NiO species.

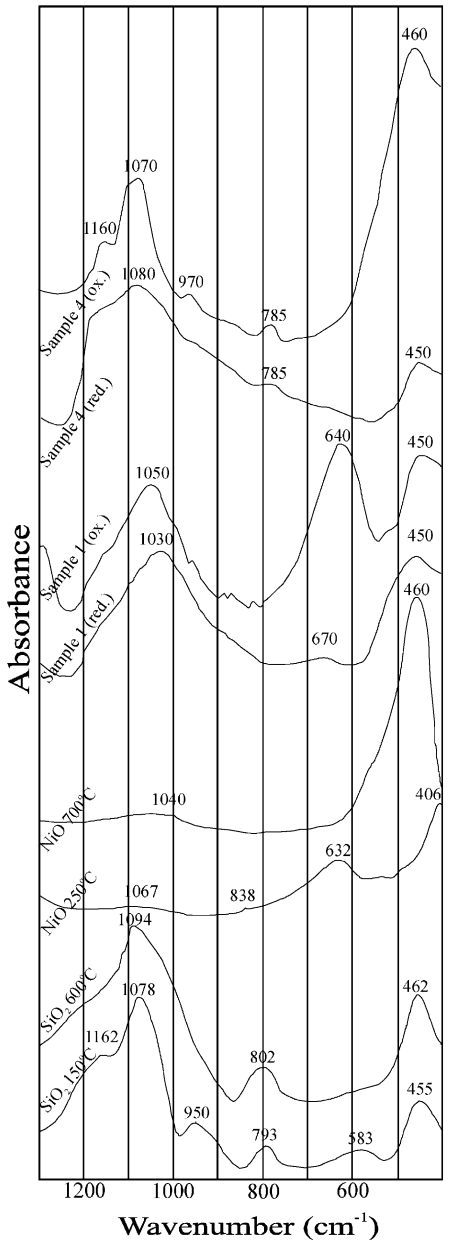

Fig. 4. IR spectra of Ni samples 1 and 4 at different stages of their preparation.

IR spectroscopic studies allow differences in the phase interaction in samples 1 and 4 to be revealed at various preparation stages (Fig. 4). The frequency ranges from 200 or 400 to 1300 cm^{-1} of the IR spectra are compared. This is exactly the range where changes

in the absorption profile attributed to the nickel–silica interaction are observed. Unlike the IR spectrum of SiO_2 xerogel calcined at 150 °C, the spectrum of the oxide form of sample 1 does not contain absorption bands at 583 cm^{-1} (Si–OH deformation vibrations), 950 cm^{-1} (Si–OH valence vibrations) and 793 cm^{-1} (symmetrical Si–O–Si valency vibrations of the silica skeleton) [22]. Disappearance of these bands, as well as a strong shift of the most intense absorption band at 1078–1050 cm^{-1}, argues the presence of Si–O–Ni bonds. As has been reported earlier [23,24], the band at 1100 cm^{-1} (asymmetrical Si–O–Si valency vibrations) is very sensitive to formation of silicates. Bands at 450 and 630 cm^{-1}, which are attributed to deformation vibrations of the silica skeleton and –O–H group of the hydrated nickel oxide, respectively, remain at the same positions. Therefore, one can assume that all silica (introduced in the form of the polysiloxane film) is involved in the chemical interaction with the surface of the dispersed NiO to form silicates. Absorption bands at 665 and 1050 cm^{-1} appeared in the spectra of nickel–silica samples are attributed to the strong chemical interaction and to formation of a new chemical compound [25]. The band at 1100 cm^{-1} is shifted to 1050 cm^{-1} due to the formation of poorly crystalline 1:1 phyllosilicate (nepouite) [26,27]. It is seen from the IR spectrum of the reduced sample 1 that the silicates formed upon mixing the constituents do not disappear despite rather high temperature of reduction in hydrogen (500 °C). The fact that the main silica band (at 1094 cm^{-1}) is shifted to 1030 cm^{-1} and a band appears at 670 cm^{-1} leads to conclusion on transformation of the unstable nepouite-like silicate species into more stable talc-like species [27].

The IR spectrum of the oxide form of sample 4 looks like a superposition of spectra of SiO_2 (150 °C) and NiO (700 °C), the absorption bands characteristic of deformation vibrations of SiO_2 and valence vibrations of NiO (455 and 460 cm^{-1}, respectively) being superimposed one on another to merge into one very intense band. The band at 1078 cm^{-1} attributed to asymmetrical valence vibrations in this SiO_2 sample is slightly shifted to lower frequencies (1070 cm^{-1}) that may mean weak interaction at the interface. The IR spectrum recorded with sample 4 reduced at 500 °C becomes similar to that of SiO_2 (600 °C) that indicates minor interaction between the constituents. This conclusions are in agreement with the inferences drawn from analysis of TPR profiles of these samples.

Differential dissolution data confirm the presence of silicates in sample 1. There are synchronous peaks in the stoichiogram (Fig. 5) indicating dissolution of a chemical compound. The Ni/Si ratio in the compound equal to 1.5 corresponds to the nepouite stoichiometry comprised in the amount not more than 2% of the sample weight. As to sample 4, silicates was not detected during the dissolution.

Micrographs of catalysts 1 and 4 (Fig. 6) were recorded after the samples have been exposed to the reaction methane medium for 30 min. As soon as the catalyst with any proportion of the support is exposed to methane, metal particles become more fluid under the action of carbon dissolved therein and can merge into larger particles [28]. For this reason, initially dispersed catalyst 1 free of coarse particles is capable of producing both thin and thick carbon filaments (Fig. 6a). It is seen that some of fine particles produce carbon filaments but others are encapsulated in

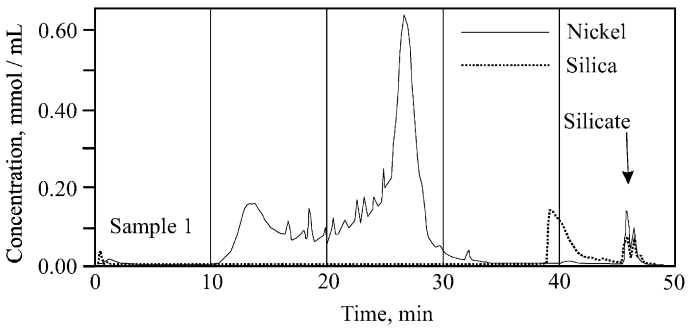

Fig. 5. Differentiating dissolution stoichiogram of reduced catalyst 1.

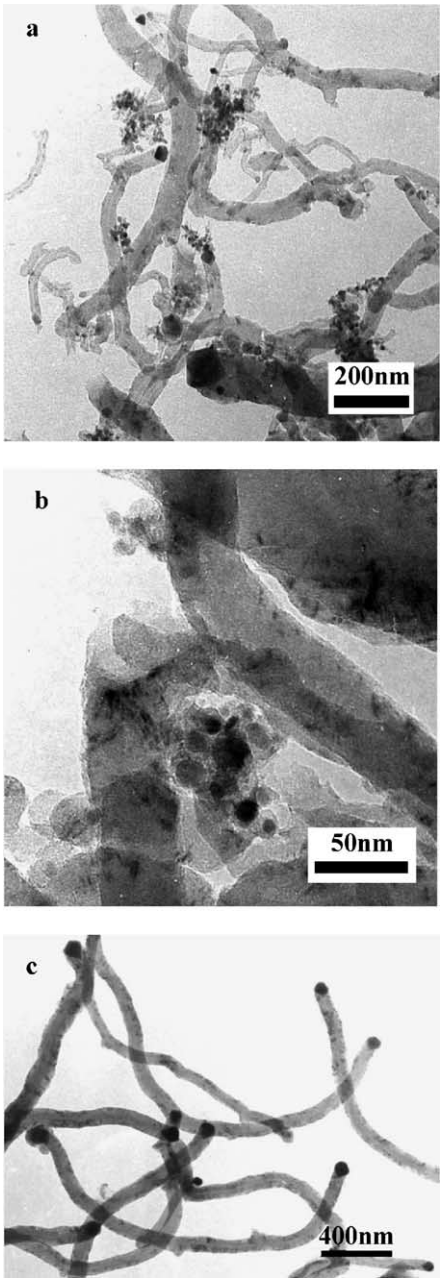

Fig. 6. Electron micrographs of Ni catalyst 1 after exposure to methane for 30 min at 550 °C (a), fine Ni particles of catalyst 1, covered with carbon (b) and Ni catalyst 4 after exposure to methane for 30 min at 550 °C (c).

carbon, the latter being much larger in number. These are the particles in the catalyst that are responsible for the low carbon yield. Unlike catalyst 1, catalyst 4 produces carbon filaments of approximately equal diameters (Fig. 6b) corresponding to the size of particles of the reduced catalyst (Fig. 2d). Nickel particles at the filament tips are well faceted crystals which take their shape under the action of the reaction medium. Encapsulated nickel particles are not seen in the micrograph (Fig. 6b). Thus, the reason for the rapid deactivation of catalyst 1 is that silicates dissolved in nickel in amount of 2 wt.% hinder rearrangement of nickel particles to form faces which are necessary for growth of filamentous carbon. As a result, nickel particles are encapsulated in carbon during the earliest hours of the reaction.

3.2. Iron catalysts

The behavior of iron catalysts during methane decomposition was the subject of our earlier study [17]. The carbon yield attained 17 g C/g Fe over unsupported iron powder. Addition of supports, except SiO_2, to the iron catalysts was established not to affect the carbon yield against the yield observed with iron alone (Fig. 7). Therefore, it was interesting to study in more detail of α-Fe–SiO_2 systems during reduction and carbonization.

A number of iron catalysts with the same silica content (10 mass%) but different specific surface area of initial Fe_2O_3 are characterized in Table 2 (first series of the catalysts). The average size of iron particles is seen to be almost equal in all the reduced catalysts but the carbon yields different. A surprising fact is that the carbon yield is 10.5 g C/g Fe over sample 6 prepared from the most inert iron oxide (4 m^2/g specific

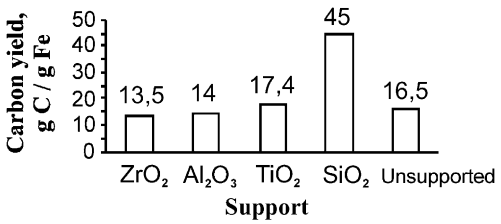

Fig. 7. Influence of the chemical nature of the support on carbon yield (content of Fe in catalysts was 85 wt.%, reaction temperature was 700 °C).

Table 2
Influence of the specific surface area of Fe_2O_3 on carbon yield over corresponding 90% Fe–10% SiO_2 catalysts. Temperature of reduction and reaction is 700 °C

Sample	Specific surface area of Fe_2O_3 (m^2/g)	Average size of Fe_2O_3 particles by XRD (nm)	Average size of Fe particles by XRD (nm)	Average size of Fe particles after 1 h in methane by XRD (nm)	Carbon yield (g C/g Fe)
1	106	Amorphous	50	29	22.5
2	61	30	57	24	30
3	29	33	57	25	30
4	19	45	57	27	30
5	9	90	67	31	26.5
6	4	>100	67	35	10.5

surface area), whereas it reaches 16.5 g C/g Fe over the reduced silica-free sample [17], i.e. the inhibiting effect of silica takes place. An increase in the contact area between iron oxide and silica (samples 1–5) gives rise to a higher carbon yield compared to the yield over iron powder, i.e. this is the case of promoting effect of silica. Thus, the only reason for the difference in carbon yield observed with various 90% Fe–10% SiO_2 catalysts is the presence of silicate species capable of either inhibit or promote the process of formation of filamentous carbon depending on their proportion in the catalyst.

In order to support this conclusion, another series of iron–silica catalysts was studied. These were catalysts prepared from Fe_2O_3 with specific surface area equal to 29 m^2/g but containing different amount of silica (second series). Comparative TPR profiles recorded during reduction of these samples and the unsupported Fe_2O_3 are shown in Fig. 8. There are two peaks of hydrogen consumption in the TPR profile of the unsupported oxide; the first one is attributed to the $Fe_2O_3 \rightarrow Fe_3O_4$ transition, and the second to complete reduction of iron oxides to α-Fe in accordance with literature data [29]. Introduction of silica results in a pronounced shift of completion of the reduction towards the range of higher temperatures. Iron oxides are known [30] to be inclined to strong interactions with SiO_2. An increase in the silica proportion in the catalyst results in separation of the stages of oxide species reduction. The reduction is seen to be far from completion at 700 °C for all the samples except the unsupported iron oxide. At the same time, only peaks of α-Fe but no line of iron oxide are seen in XRD patterns recorded for all the samples. The remained unreduced silicate species are X-ray amorphous and, for this reason, not detected, while

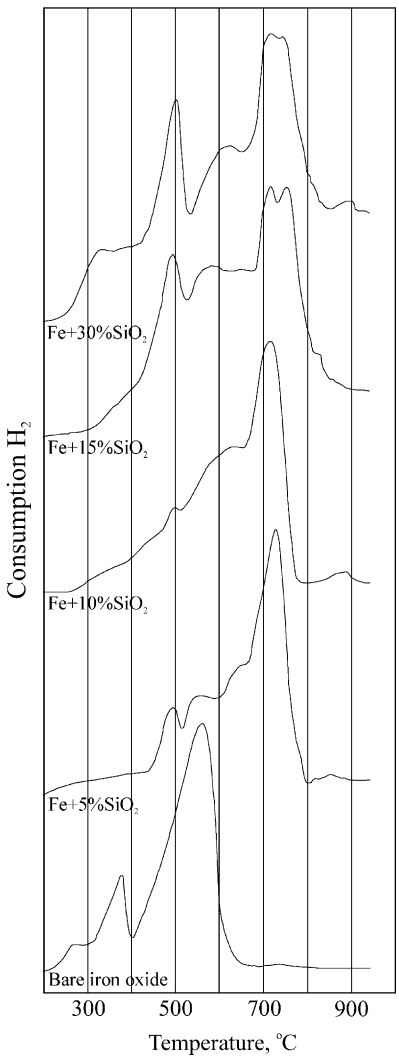

Fig. 8. TPR profiles, obtained by reduction of Fe_2O_3/SiO_2 systems.

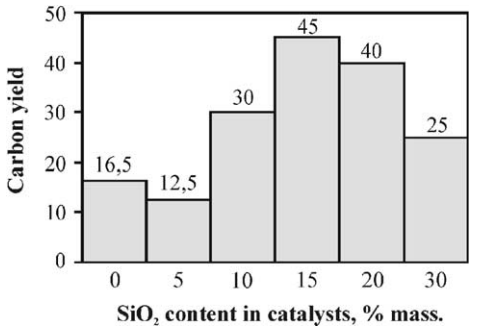

Fig. 9. Carbon yield (g C/g Fe) as a function of content of SiO_2 in iron–silica catalysts (iron oxide with specific surface area equal to 29 m^2/g was used for the preparation of catalysts). Methane decomposition temperature was 700 °C.

the presence of them is indicated by pertinent TPR profiles, where extended tails of peaks or not high maxima of hydrogen consumption are observed at temperatures up to 900 °C. Thus, all reduced samples, except iron powder prepared from unsupported iron oxide, contain silicate species. Fig. 9 illustrates how the silica content affects the yield of carbon during methane decomposition. Similar to the first series of catalysts, this one includes one sample providing a lower carbon yield (12.5 g C/g Fe) than unsupported iron powder (16–17 g C/g Fe) [17]. This is the sample containing 5% of silica. In the first series, the lowest carbon yield (10.5 g C/g Fe) is observed with sample 6. Presumably, silicate species are comprised in the lowest proportions in these samples; for the former this is due to the lowest proportion of silica (5 wt.%) and for the latter due to the low specific surface area of Fe_2O_3 which is low reactive with respect to silica. The next catalyst under consideration is the sample containing 30% of silica. There is evidently the highest proportion of silica in this sample, and the carbon yield provided by it (25 g C/g Fe) is comparable to the yield observed with sample 1 (22.5 g C/g Fe, Table 2) which was prepared using hematite with the largest specific surface area (106 m^2/g) to make the interaction with silica easier. Thus, we have two boundary points of the carbon yield in both catalyst series. It is evident that they correspond to the lowest and the highest proportion of silicate species in the samples. The samples providing the maximal carbon yield (up to 45 g C/g Fe) are at the intermediate positions. It can be assumed that the amount

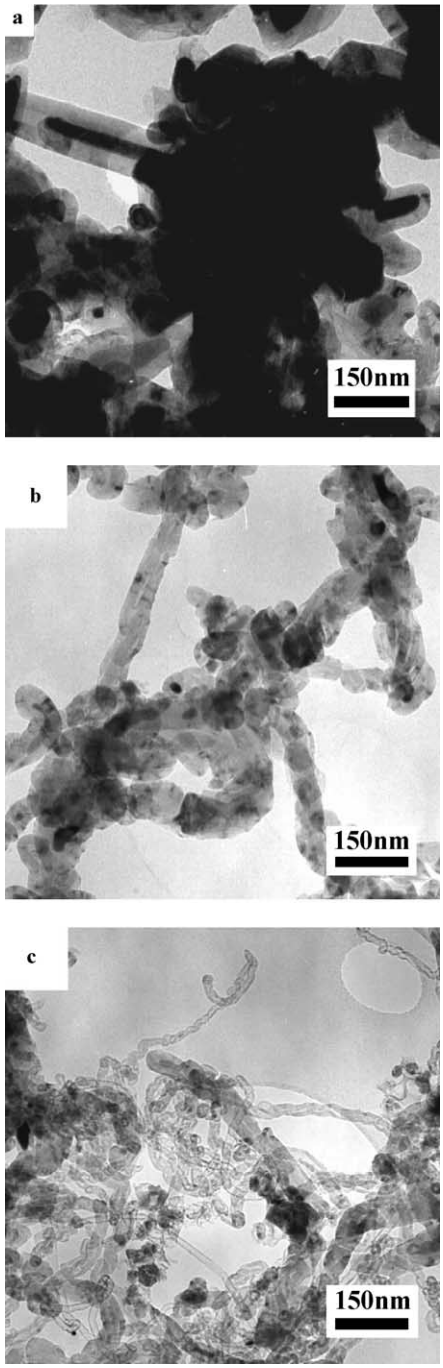

Fig. 10. Electron micrographs of Fe/SiO_2 catalyst: 1 h in methane (a), 6 h in methane (b), full carbonization (c). Temperature of the reaction was 700 °C.

of carbon produced by the catalyst depends on the amount of silicate remaining after reduction. The silicates can either inhibit or promote the process. The proposed hypothesis needs further studies by analytic methods.

Silicate species comprised in the catalyst can either extend or shorten the lifetime of the catalyst but, eventually, the catalyst is irreversibly deactivated in any case. Fig. 10a–c illustrates different phases of evolution of the Fe–SiO_2 catalyst exposed to methane. During the first hour of the reaction, iron-carbide particles undergo intensive dispersing by carbon growing thereon (Fig. 10a). The metal, like a fluid, is drawn into the hollow carbon tubes. The pattern changes in a while; there is no continuous catalyst body but all the particles are at the tips of or inside the filaments (Fig. 10b). Facetted metal particles, which are ample during carbonization of nickel samples (Fig. 6a–c), are not observed. As soon as the catalyst looses completely its activity, the carbon filaments become thinner and thin-wall tubes appear (Fig. 10c). The metal particles are few in number and encapsulate in the carbon filaments. These observations reveal that iron catalysts are deactivated due to disintegration and encapsulation of the iron particles in the course of carbon growth.

4. Conclusions

Evolution of Ni/SiO_2 and Fe/SiO_2 catalysts for decomposition of methane at various stages of catalyst preparation and during the reaction was studied using a number of physicochemical methods.

The carbon yield is demonstrated to depend only on the interaction between nickel and silica. The presence of silicates in amount of ∼2 wt.% in the 90% Ni–10% SiO_2 catalyst gives rise to a rapid catalyst deactivation (the carbon yield is 40 g C/g Ni). The carbon yield as high as 384 g C/g Ni is observed with silicate-free 90% Ni–10% SiO_2 catalyst.

It is assumed that silicate can either inhibit or promote formation of carbon depending on their amount comprised in Fe/SiO_2 catalysts.

Evolution of carbon morphology that results in formation of thin-wall carbon nanotubes is shown to occur during decomposition of methane over Fe/SiO_2 catalysts.

Acknowledgements

The authors are grateful to Dr. G.N. Kustova for IR spectroscopic studies, to Dr. A.L. Chuvilin for TEM studies, to Dr. V.V. Malakhov and L.S. Dovlitova for differential dissolution studies.

References

[1] G.G. Kuvshinov, Yu.I. Mogilnykh, D.G. Kuvshinov, V.N. Parmon, S.G. Zavarukhin, Proceedings of the 11th World Hydrogen Energy Conference, Stuttgart, 1996, pp. 2–6 (Abstract).
[2] T. Zhang, M.D. Amiridis, Appl. Catal. A 167 (1998) 161.
[3] R.T.K. Baker, M.A. Barber, P.S. Harris, F.S. Feates, R.J. Waite, J. Catal. 26 (1972) 51.
[4] V.B. Fenelonov, V.A. Likholobov, A.Yu. Derevyankin, M.S. Mel'gunov, Catal. Today 42 (1998) 341.
[5] N.M. Rodriguez, J. Mater. Res. 8 (1993) 3233.
[6] W.L. Holstein, J. Catal. 152 (1995) 42.
[7] L. Kepinski, Carbon 30 (1992) 949.
[8] V.B. Fenelonov, L.B. Avdeeva, V.I. Zheivot, L.G. Okkel, O.V. Goncharova, L.G. Pimneva, Kinet. Katal. 34 (1993) 545.
[9] V.V. Molchanov, V.V. Chesnokov, R.A. Buyanov, N.A. Zaitseva, Kinet. Katal. 39 (1998) 407.
[10] G.G. Kuvshinov, Yu.I. Mogilnykh, M.Yu. Lebedev, Direct oxidation of hydrogen sulfide to sulfur over filamentary carbon, Division of Fuel Chemistry Preprints of Symposia, vol. 43, No. 4, American Chemical Society, August 1998, p. 846.
[11] N.M. Rodriguez, M.S. Kim, R.T.K. Baker, J. Phys. Chem. 98 (1994) 13108.
[12] Sh.K. Shaikhutdinov, L.B. Avdeeva, B.N. Novgorodov, V.I. Zaikovskii, D.I. Kochubey, Catal. Lett. 47 (1997) 35.
[13] A. Chambers, C. Park, R.T.K. Baker, N.M. Rodriguez, J. Phys. Chem. B 102 (1998) 4254.
[14] M.S. Kim, N.M. Rodriguez, R.T.K. Baker, J. Catal. 131 (1991) 60.
[15] M.A. Ermakova, D.Yu. Ermakov, G.G. Kuvshinov, L.M. Plyasova, J. Catal. 187 (1999) 77.
[16] L.B. Avdeeva, D.I. Kochubey, Sh.K. Shaikhutdinov, Appl. Catal. A 177 (1999) 43.
[17] M.A. Ermakova, D.Yu. Ermakov, A.L. Chuvilin, G.G. Kuvshinov, J. Catal. 201 (2001) 183.
[18] M.A. Ermakova, D.Yu. Ermakov, G.G. Kuvshinov, Appl. Catal. A 201 (2000) 61.
[19] V.V. Malakhov, A.A. Vlasov, Kinet. Catal. 36 (4) (1995) 460.
[20] B. Mile, D. Stirling, M.A. Zammit, A. Lovell, M. Webb, J. Catal. 114 (1988) 217.
[21] S.D. Robertson, B.D. McNicol, J.H. de Baas, S.C. Kloet, J.W. Jenkins, J. Catal. 37 (1975) 424.
[22] J.C. Ro, I.J. Chung, J. Non-Cryst. Solids 130 (1991) 8.
[23] A.N. Lasarev, Oscillation Spectra and Structure of Silicates, Nauka, Leningrad, 1968.

[24] V.A. Sviderskiy, M.G. Voronkov, V.S. Klimenko, S.V. Klimenko, Zh. Pricl. Chim. 70 (1997) 1698.
[25] V.A. Dsisko, S.P. Noskova, L.G. Karakchiev, M.S. Borisova, V.D. Bolgova, T.Ya. Tyulikova, Kinet. Katal. 13 (1972) 366.
[26] O. Clause, M. Kermarec, L. Bonneviot, F. Villain, M. Che, J. Am. Chem. Soc. 114 (1992) 4709.
[27] M. Kermarec, J.Y. Carriat, P. Burattin, M. Che, A. Decarreau, J. Phys. Chem. 98 (1994) 12008.
[28] M.A. Ermakova, D.Yu. Ermakov, L.M. Plyasova, G.G. Kuvshinov, Catal. Lett. 62 (1999) 93.
[29] H. Jung, W.J. Thomson, J. Catal. 128 (1991) 218.
[30] C.R.F. Lund, J.A. Dumesic, J. Catal. 72 (1981) 21.